TEAM 35

Application of reefing to high-powered rocket recovery

EPFL Rocket Team – Team 35

Project Matterhorn

Spaceport America Cup – June 19 - 23, 2018

Mission overview

Project Matterhorn

TEAM 35

Mission overview

Objectives

TEAM 35

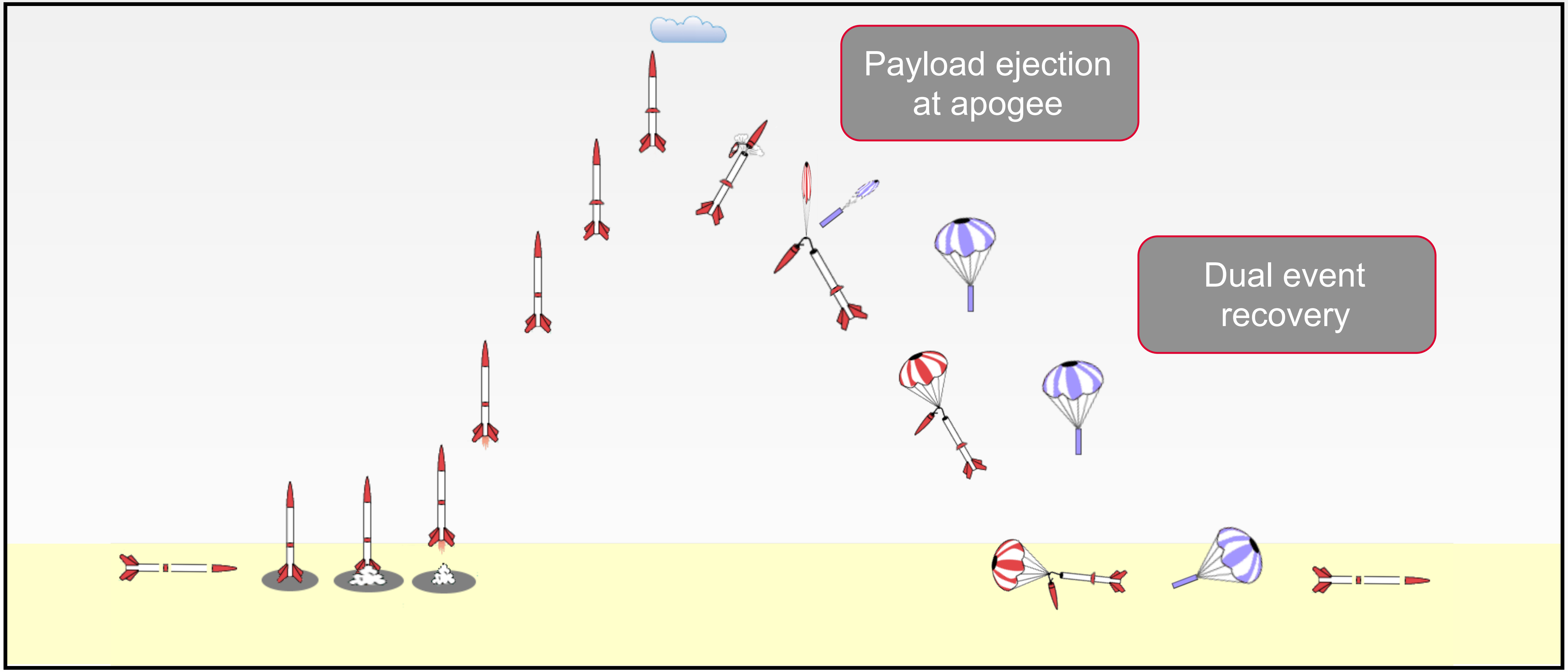

Mission overview

TEAM 35

System overview

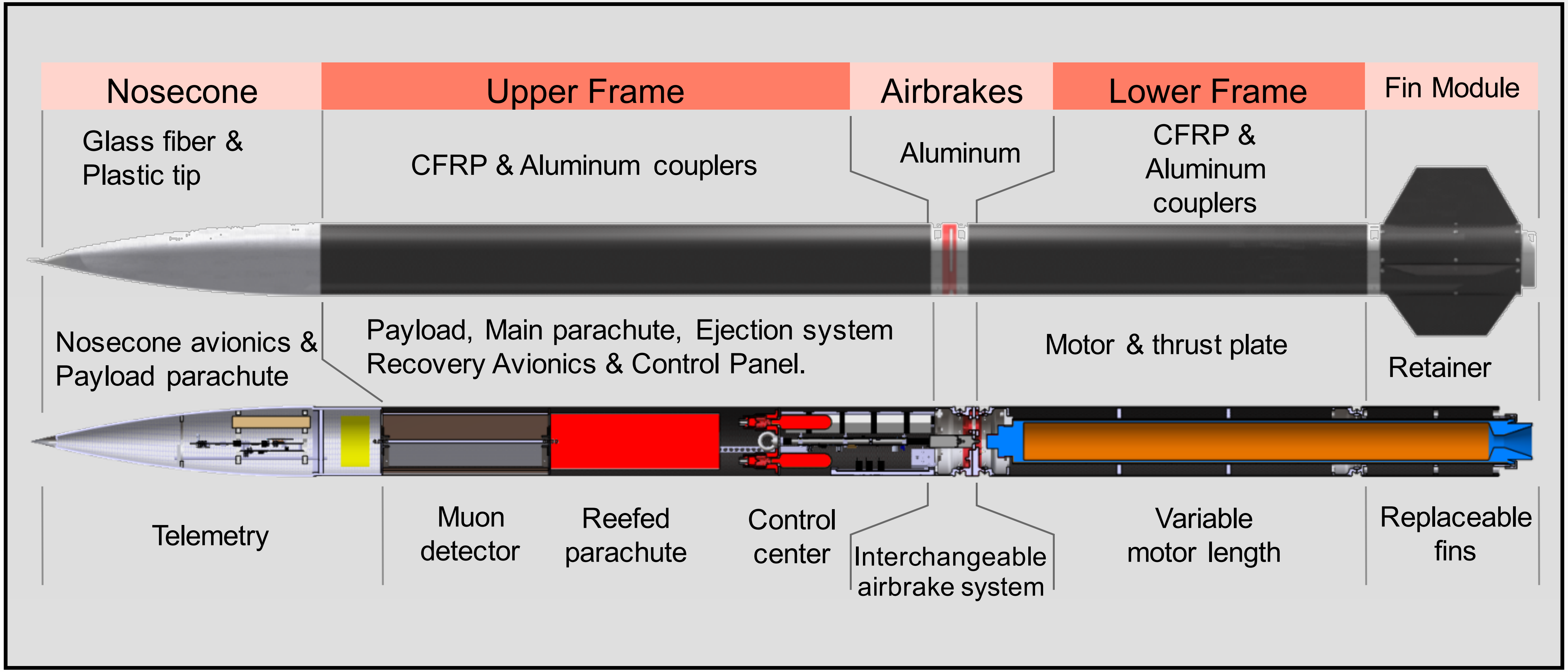

Reefing

Introduction

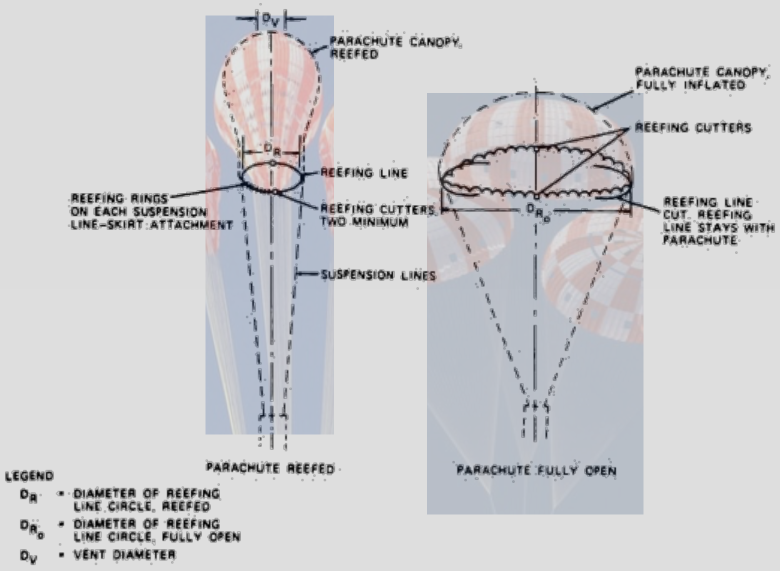

FIGURE 5-66. Parachute Skirt Reefing.

Reefing

Implementation

TEAM 35

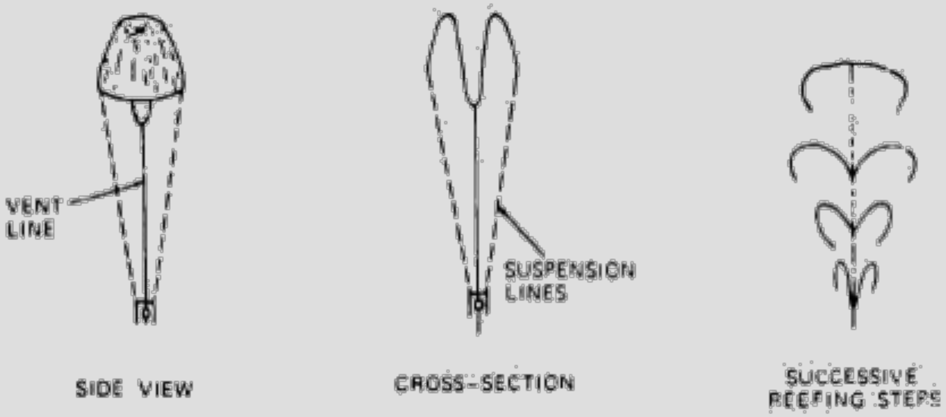

FIGURE 5-68. Parachute Vent Reefing.

Parachute design

Retractation response shaping

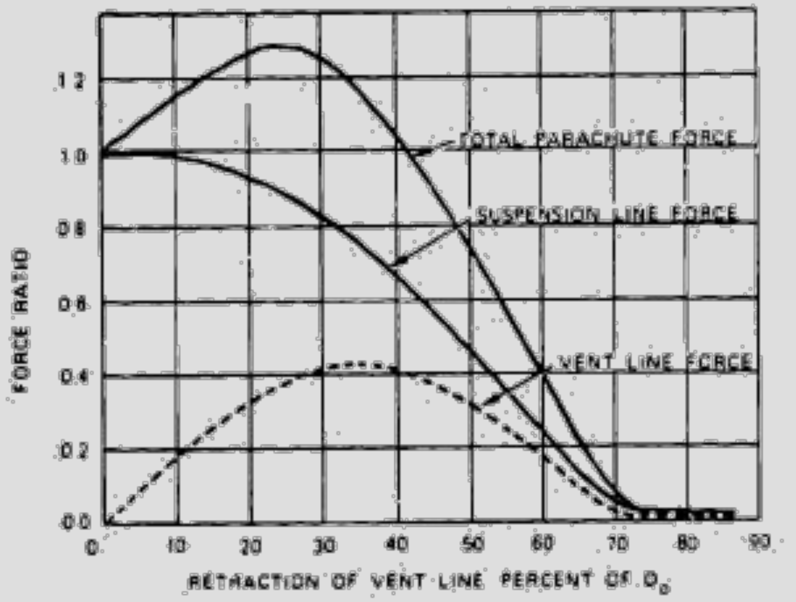

FIGURE 5-69. Total Parachute Force, Suspension-Line Force, and Vent-Line Force, as Functions of Vent-Line Retraction.

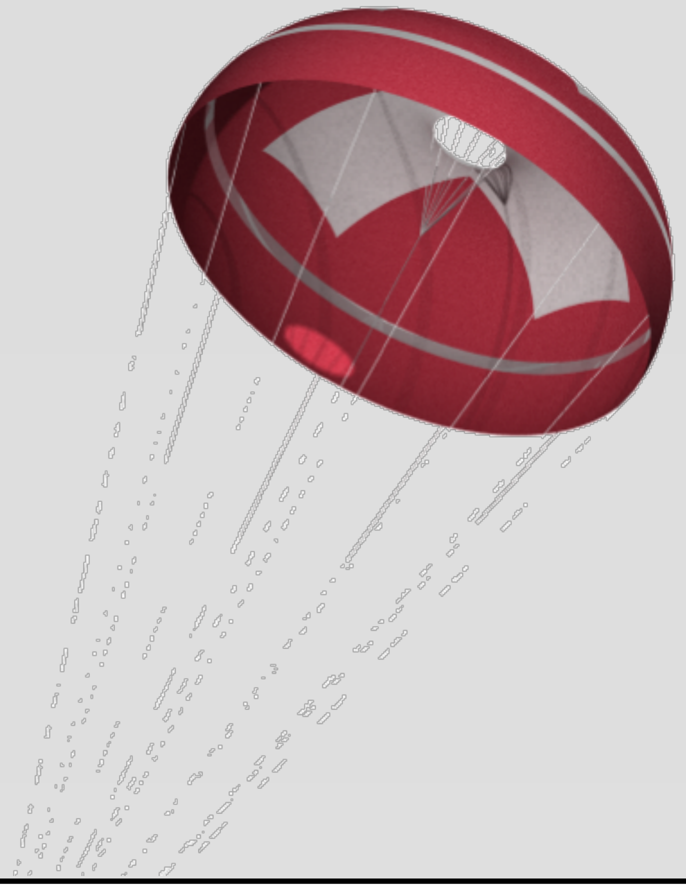

Parachute design

Stability

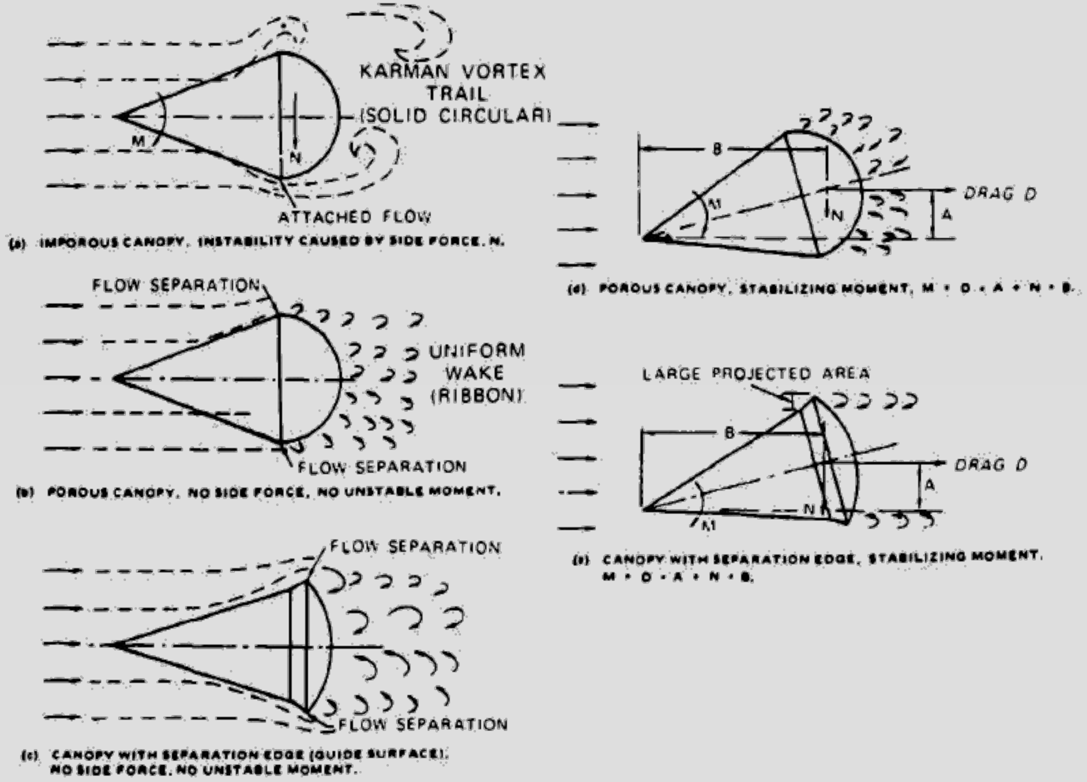

FIGURE 5-32. Relationship of Airflow and Stability for Various Parachutes.

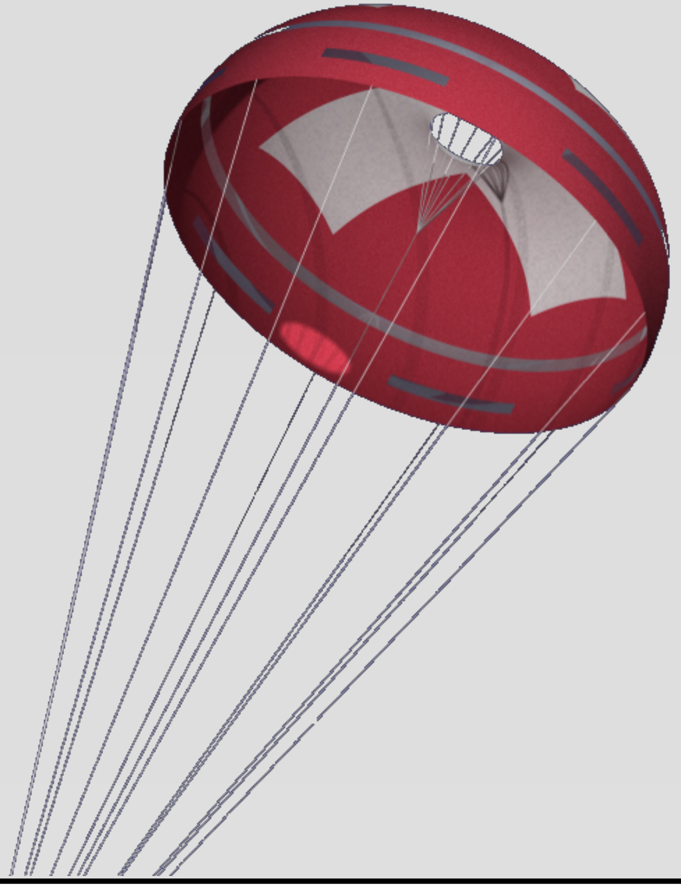

Parachute design

Lines length

TEAM 35

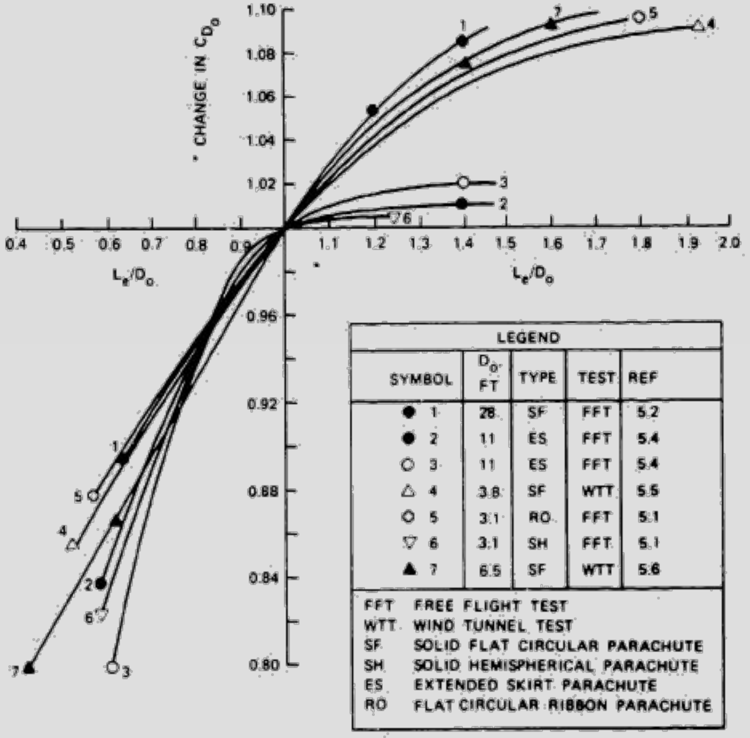

FIGURE 5-20. Variation of Drag Coefficient With Suspension-Line Ratio for Several Parachute Types.

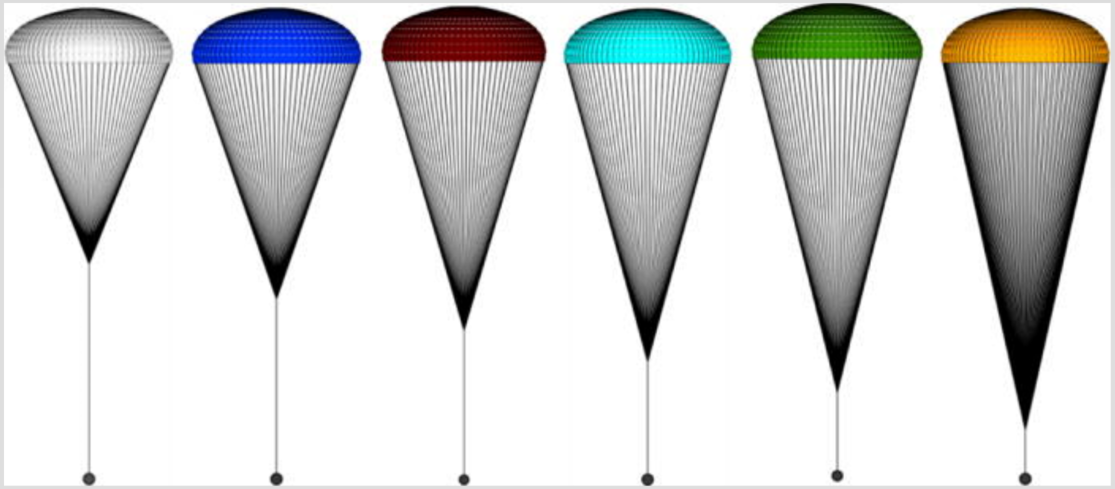

Parachute configurations with suspension line length ratios of 1.00, 1.15, 1.30, 1.44, 1.60, and 1.76

Line-cutter

TEAM 35

Reefing module & Shock cord

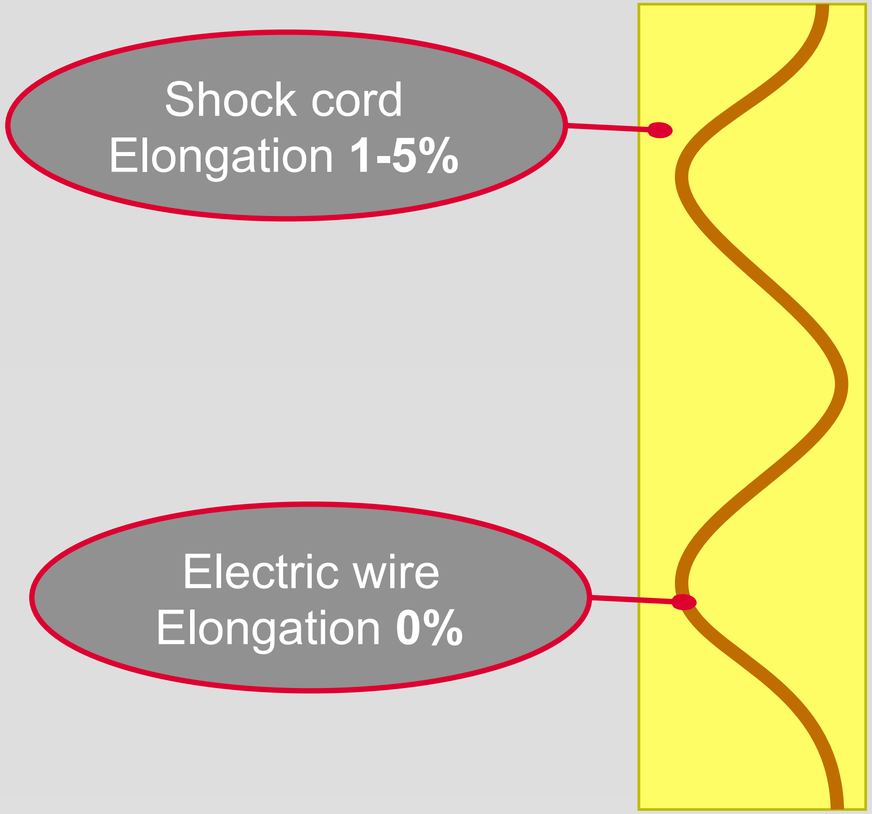

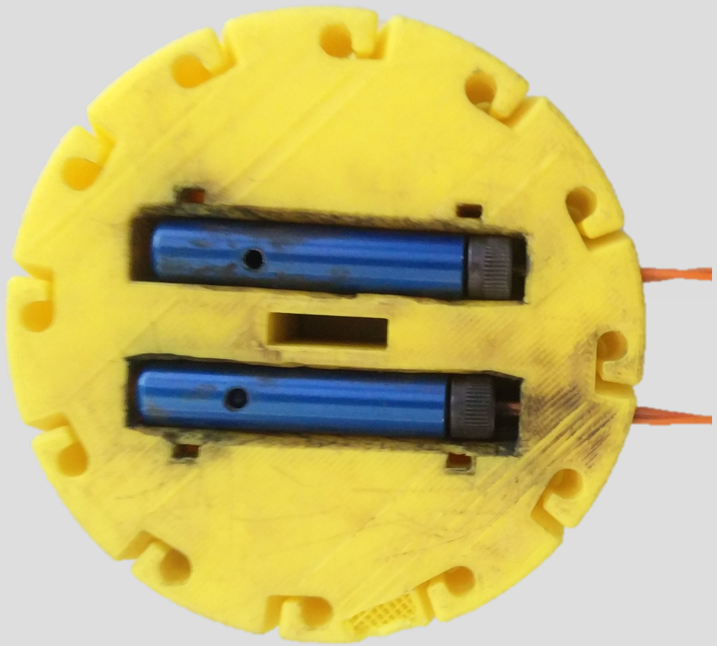

Manufacturing

Sewing

TEAM 35

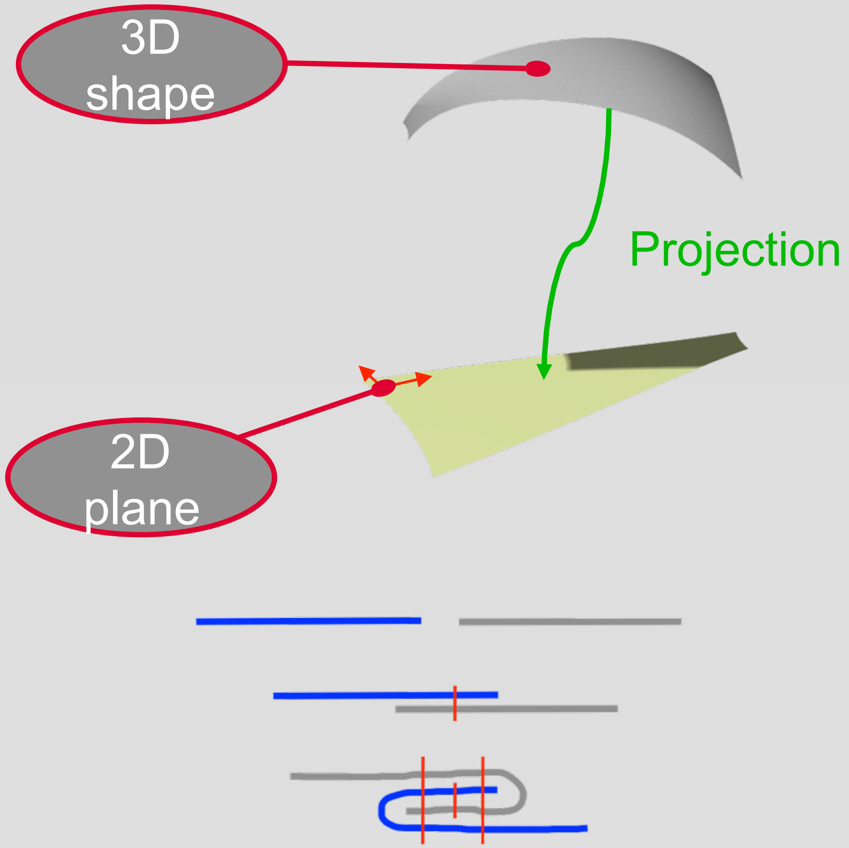

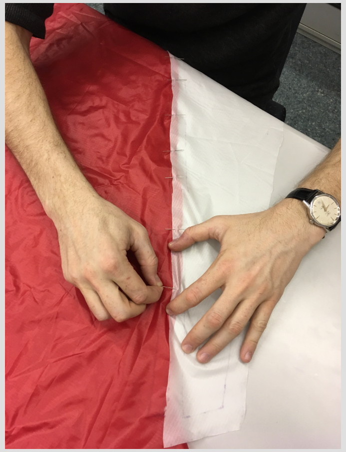

Characterization

Wind tunnel

TEAM 35

- Measured drag coefficient : $C_D \in [1.6\,, 1.8]$
- Scaling : $(C_D S) \cdot \frac{\rho\, v^2}{2} = \mathrm{mg} \xRightarrow[\substack{v=4.5\,\frac{m}{s} \\ m=15\,kg}]{} S = 6.8\ m^2$

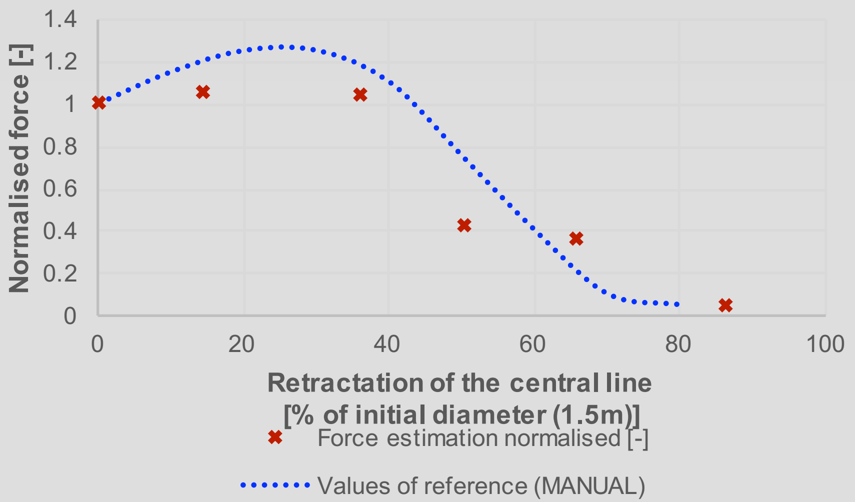

Concept of Operations

Ejection

TEAM 35

Cone ejection	Payload parachute inflation	Reefed parachute inflation
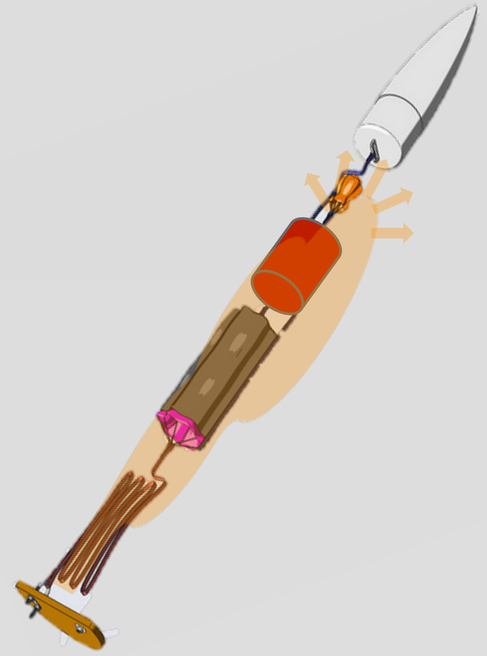	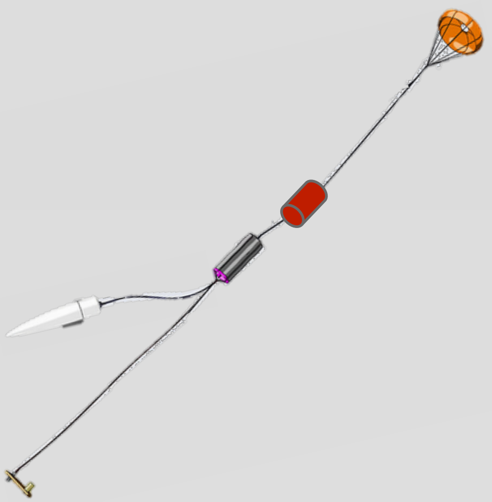	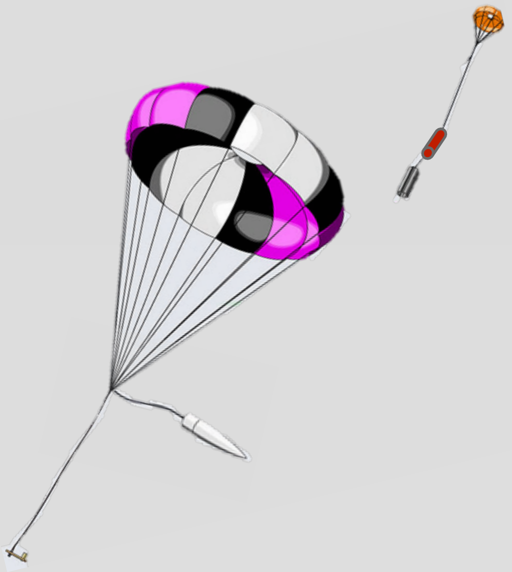
CO2 cartridge opening	Payload’s parachute pull the main chute out	Main parachute is pulled out the deployment bag and inflates

Characterization

Drop test

TEAM 35

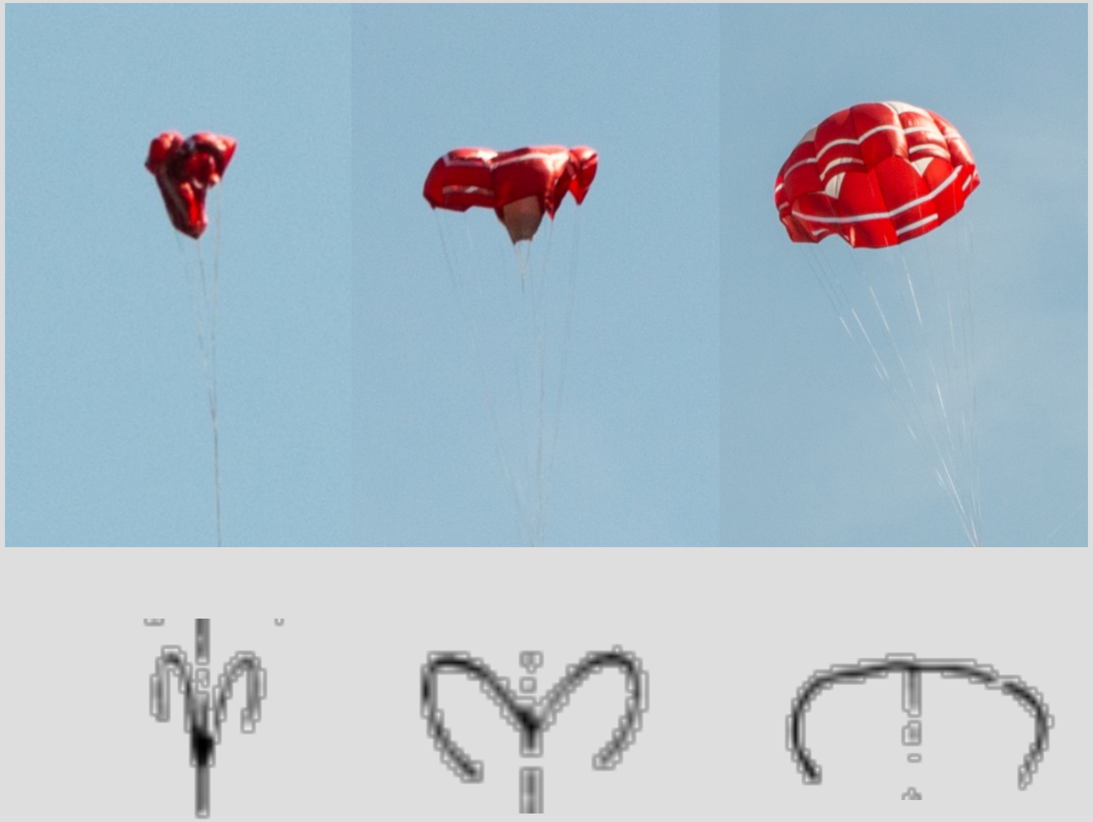

Validation of concept

Matterhorn I

TEAM 35

Validation of concept

Matterhorn I

TEAM 35

Validation of concept

TEAM 35

Results

Characterization

Maximum opening force

TEAM 35

$$\boldsymbol{F = (C_D S)_{p-r} \cdot q_2 \cdot C_x \cdot X_1 = \begin{cases} 1088[N]\ ;\ \ with\ Planz \\ 940.5[N]\ ;\ with \left[\frac{W}{(C_D S)_p}\right] \end{cases}}$$

with,

$(C_D S)_{p-r} = 8.93[\mathrm{m}^2]$; $the\ relative\ active\ drag\ area$

$q_2 = 260.0[\mathrm{Pa}]$; $the\ dynamic\ pressure$

$C_x = 1.35\ [-]$;
$the\ coefficient\ of\ opening\ force\ at\ infinite\ mass$

X_1 ; $the\ opening\ force$ reduction factor

$$X_{1,Pflanz} = X_{1,\frac{W}{C_D S}} = 0.3[-]$$

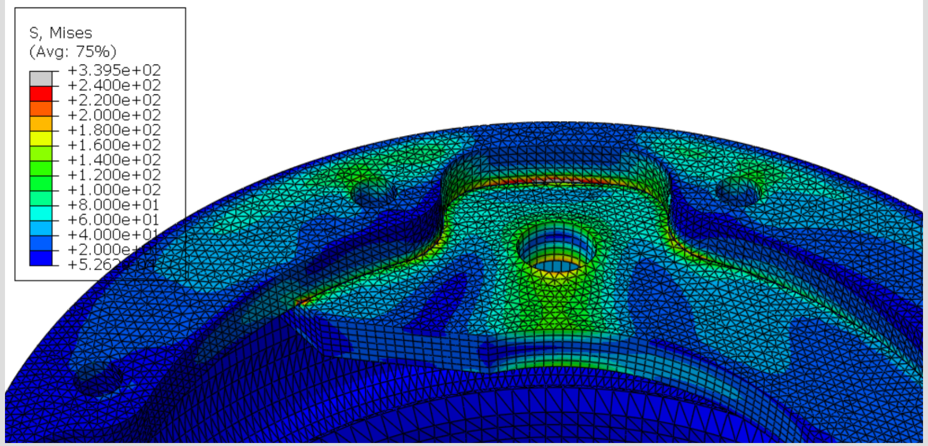

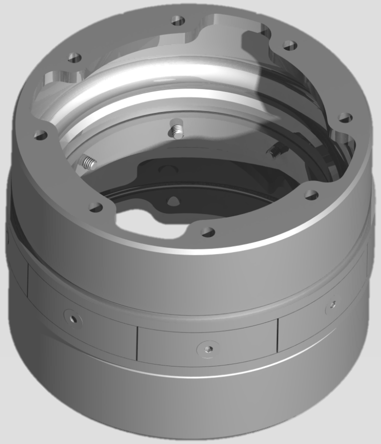

Characterization

TEAM 35

Drop test

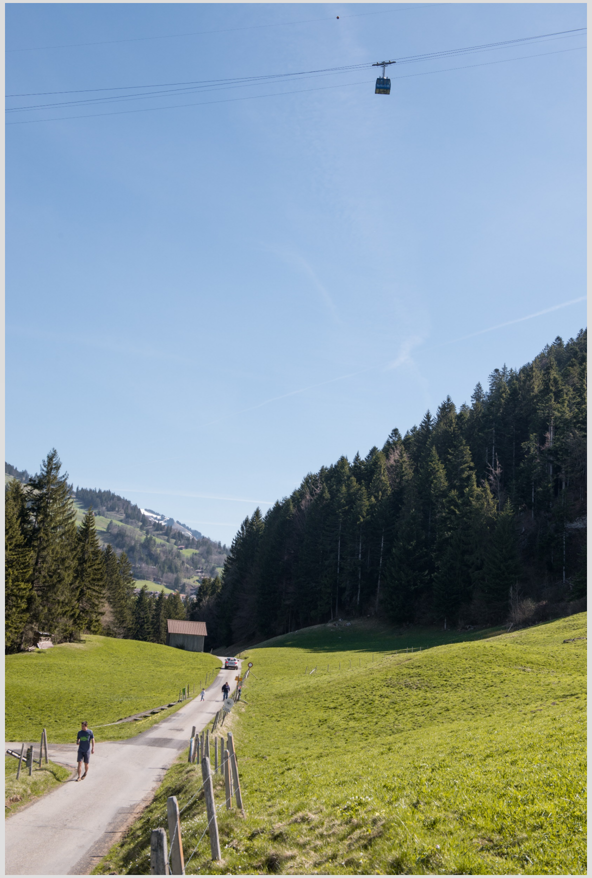

Questions ?

TEAM 35

EPFL Rocket Team is proud to be supported by :

Together ahead. RUAG

evs

LEMO The Original Push-Pull Connector

CHATEAU DE FERRAND
GRAND CRU CLASSÉ DE SAINT-EMILION

suter-kunststoffe ag
swiss-composite.ch

sta TRAVEL

SAUBER Aerodynamics

KIFA

PB SWISS TOOLS

FORUM EPFL

BIC

FAULHABER

OPTIONS

Peacock Solutions

espace montage

innovaud

swiss space center

KUEHNE+NAGEL

References

TEAM 35

- Unknown author, **pxhere.com** – Picture (slide 2) Unknow author, **nasa.gov** – Pictures (slide 5)
- **T.W. Knacke**, *Parachute Recovery Systems Design Manual* – Figure (Slide 5, 6, 7, 8, 9, 14)
- **Tequesquitengo** – Pictures (slide 6)
- **K. Takizawa, T. Spielman, C. Moorman and T.E. Tezduyar,** Fluid-Structure Interaction Modeling of Spacecraft Parachutes for Simulation-Based Design, *J. Appl. Mech* 79(1) – Pictures (slide 9)
- Based on drawings found on **eurocketry.org** – Drawing (slide 13)
- Screenshot on **Google Maps** – map (slide15)

Appendix

Opening force computation

TEAM 35

Dynamic pressure :

$$q_r = \frac{\rho}{2} \cdot \frac{\sigma_r}{\sigma_0} \cdot v_r^2 \ ; \ q_0 = \frac{\rho}{2} \cdot \frac{\sigma_0}{\sigma_0} \cdot v_m^2$$

Equivalent active drag surface :

$$(C_D S)_r = \frac{W_d}{q_r} \ ; \ (C_D S)_p = \frac{W_d}{q_0}$$

$$(C_D S)_{p-r} = (C_D S)_p - (C_D S)_r$$

Planz method

$$A_r = \frac{2W_d}{(C_D S)_{p-r} \cdot \rho \cdot g \cdot t_{f,r} \cdot v_1} \ ; \ t_{f,m} = \frac{D_0}{v_r \cdot n_m \cdot \sqrt{\frac{(C_D S)_{p-r}}{(C_D S)_p}}}$$

$$F_{m,Pflanz} = (C_D S)_{p-r} \cdot q_2 \cdot C_x \cdot X_{1,m,\mathrm{Pflanz}}$$

$$\tilde{F}_{m,Pflanz} = F_{r,Pflanz} + W_d$$

$\left[\frac{W}{(C_D S)_p}\right]$ ***method***

$$\left[\frac{W}{(C_D S)_p}\right]_m = \frac{W_d}{(C_D S)_{p-r}}$$

$$F_{r,\frac{W}{C_D S}} = (C_D S)_{p-r} \cdot q_2 \cdot C_x \cdot X_{1,m,\frac{W}{C_D S}}$$

Appendix

Opening force factor

TEAM 35

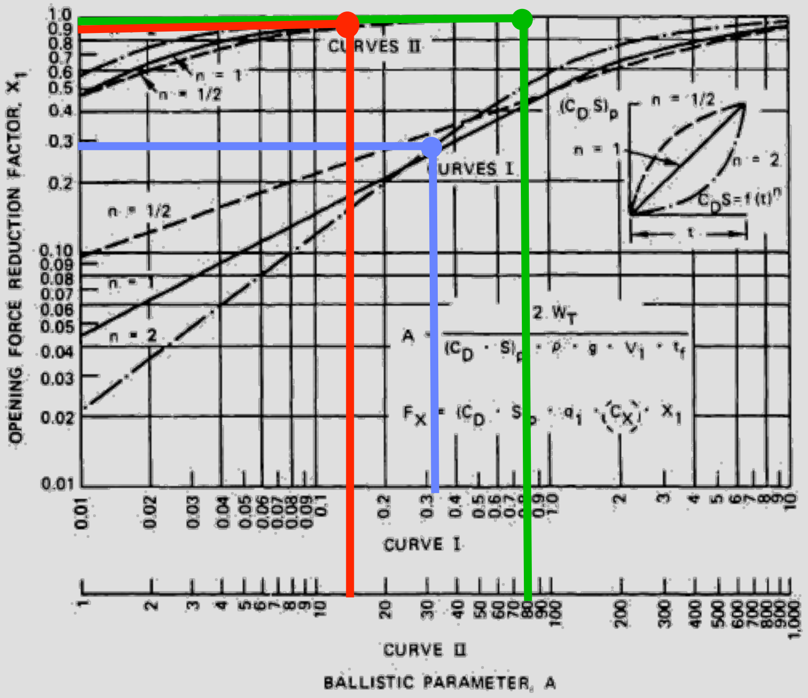

FIGURE 5-51. Opening-Force Reduction Factor, X_1, Versus Ballistic Parameter, A.

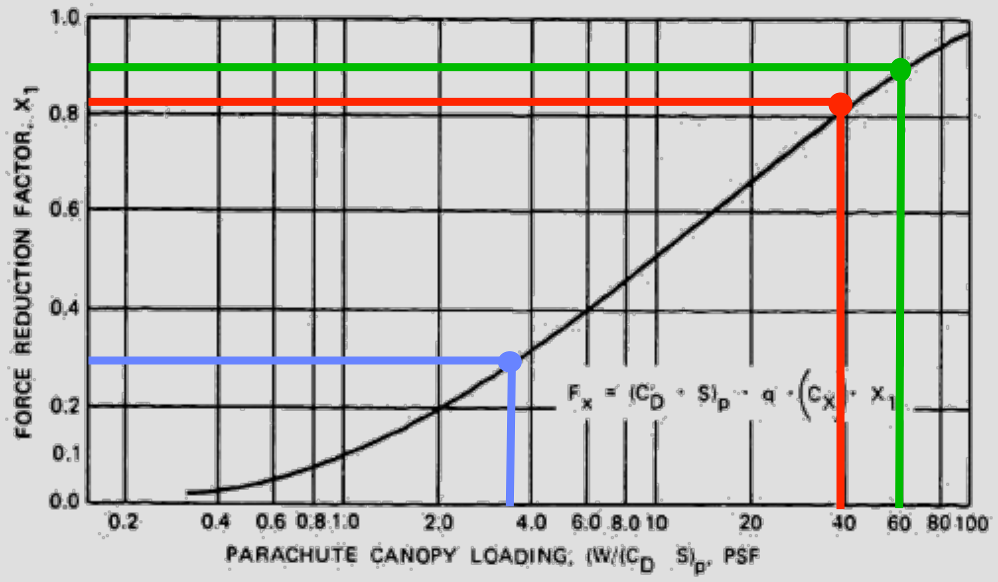

FIGURE 5-48. Opening-Force Reduction Factor Versus Canopy Loading.

Appendix

Parachute form factor

TEAM 35

TABLE 5-1. Solid Textile Parachutes.

TYPE	CONSTRUCTED SHAPE PLAN	CONSTRUCTED SHAPE PROFILE	$\frac{D_c}{D_o}$	INFLATED SHAPE $\frac{D_p}{D_o}$	DRAG COEF C_{D_o} RANGE	OPENING FORCE COEF C_X (INF MASS)	AVERAGE ANGLE OF OSCILLATION, DEGREES	GENERAL APPLICATION
FLAT CIRCULAR			1.00	0.67 TO 0.70	0.75 TO 0.80	~1.7	±10 TO ±40	DESCENT, OBSOLETE
CONICAL			0.93 TO 0.95	0.70	0.75 TO 0.90	~1.8	±10 TO ±30	DESCENT, M < 0.5
BICONICAL			0.90 TO 0.95	0.70	0.75 TO 0.92	~1.8	±10 TO ±30	DESCENT, M < 0.5
TRICONICAL POLYCONICAL			0.90 TO 0.95	0.70	0.80 TO 0.96	~1.8	±10 TO ±20	DESCENT, M < 0.5
EXTENDED SKIRT 10% FLAT		0.1 D_c	0.86	0.66 TO 0.70	0.78 TO 0.87	~1.4	±10 TO ±15	DESCENT, M < 0.5
EXTENDED SKIRT 14.3% FULL		0.143 D_c	0.81 TO 0.85	0.66 TO 0.70	0.75 TO 0.90	~1.4	±10 TO ±15	DESCENT, M < 0.5
HEMISPHERICAL			0.71	0.66	0.62 TO 0.77	~1.6	±10 TO ±15	DESCENT, M < 0.5, OBSOLETE
GUIDE SURFACE (RIBBED)			0.63	0.62	0.28 TO 0.42	~1.2	0 TO ±2	STABILIZATION, DROGUE, 0.1 < M < 1.5
GUIDE SURFACE (RIBLESS)			0.66	0.63	0.30 TO 0.34	~1.4	0 TO ±3	PILOT, DROGUE, 0.1 < M < 1.5
ANNULAR			1.04	0.94	0.85 TO 0.95	~1.4	< ±6	DESCENT, M < 0.5
CROSS			1.15 TO 1.19	0.66 TO 0.72	0.60 TO 0.85	1.1 TO 1.2	0 TO ±3	DESCENT, DECELERATION

TABLE 5-2. Slotted Parachutes.

TYPE	CONSTRUCTED SHAPE PLAN	CONSTRUCTED SHAPE PROFILE	$\frac{D_c}{D_o}$	INFLATED SHAPE $\frac{D_p}{D_o}$	DRAG COEF C_{D_o} RANGE	OPENING FORCE COEF C_X (INF MASS)	AVERAGE ANGLE OF OSCILLATION, DEGREES	GENERAL APPLICATION
FLAT (FIST) RIBBON			1.00	0.67	0.45 TO 0.50	~1.05	0 TO ±3	DROGUE, DESCENT, DECELERATION, OBSOLETE
CONICAL RIBBON			0.95 TO 0.97	0.70	0.50 TO 0.55	~1.05	0 TO ±3	DESCENT, DECELERATION, 0.1 < M < 2.0
CONICAL RIBBON (VARIED POROSITY)				0.70	0.55 TO 0.60	1.05 TO 1.30	0 TO ±3	DROGUE, DESCENT, DECELERATION, 0.1 < M < 2.0
RIBBON[1] (HEMISFLO)			0.62	0.62	0.30[1] TO 0.46	1.00 TO 1.30	±2	SUPERSONIC, DROGUE, 1.0 < M < 3.0
RINGSLOT			1.00	0.67 TO 0.70	0.56 TO 0.65	~1.05	0 TO ±5	EXTRACTION, DECELERATION, 0.1 < M < 0.9
RINGSAIL			0.84	0.69	0.75 TO 0.86	~1.10	±5 TO ±10	DESCENT, M < 0.5
DISC-GAP-BAND			0.73	0.65	0.52 TO 0.58	~1.30	±10 TO ±15	DESCENT, M < 0.5

[1] FOR SUPERSONIC APPLICATION, SEE SECTION 5.8

Appendix

Coupler

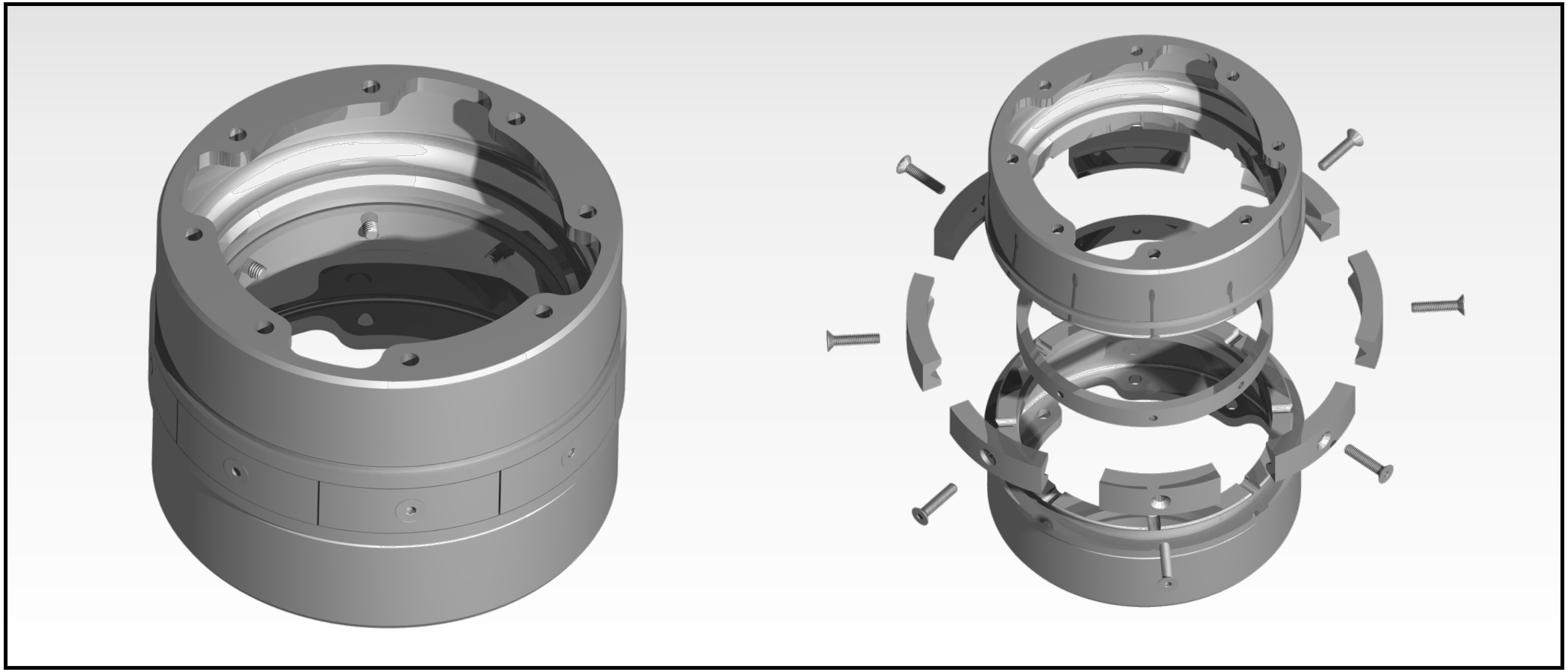

Appendix

Simulation

TEAM 35

- Assumptions :
  - Load case on one of the two rods : 4000N
  - No deformation of the carbon tube
  - Numerical instabilities at edges
- Results :
  - Maximum stress : 200 Mpa <

    $\sigma_{max,\,Al\,6082}$ = 240-350 Mpa